Optimization of a Rotor with Morphing Blades using Particle Swarm Algorithm

Stephan Benz
Mechanical and Aerospace Engg.
Technical University
Braunschweig, Germany

Rohin Kumar Majeti
Rotorcraft, Institute of Flight Systems
German Aerospace Center (DLR)
Braunschweig, Germany
Germany

ABSTRACT

A particle swarm optimization is used to investigate the optimal morphing parameters for a chord morphing rotor concept, which is developed by the German Aerospace Center (DLR) under the framework of the European project SABRE. Since the morphing parameters can be dependent on the application of the helicopter, three different missions are chosen to be observed. The particle swarm optimization is implemented and set up to solve single and multi-objective problems, defined in three scenarios. Scenario 1 covers only power, whereas scenario 2 adds tip elastic torsion and scenario 3 also includes vibratory hub loads. A two leveled particle swarm algorithm is described, to cover full missions as opposed to single velocities. The effect of missions on the optimal morphing parameters is analyzed and optimal chord morphing parameters are presented per scenario, mission and velocity. The particle swarm optimization is shown to find rotor geometries, that use less power than the baseline rotor, while keeping structural and vibrational strains within limits.

Keywords

optimization, helicopter rotor, rotor blade optimization, particle swarm algorithm, variable chord extension

INTRODUCTION

Industry is always trying to improve their products in terms of performance and economical aspects. Since a power efficient fixed geometry of rotor blade requires compromises in many different aspects like vibration and stress limits, the helicopter rotor design has not changed drastically over time. Most rotors feature rectangular blades and linear twist.

However, there is research to reduce the power consumption and optimize helicopter rotors. The optimal hovering rotor in theory has a hyperbolical chord length and twist [1] (shown in Fig. 1 and Fig. 2, adapted from [2]), which chord morphing concepts want to achieve for hover, while not being forced to keep this geometry at all times. This is necessary, since the optimal geometry at high velocities can differ from hover, which would result in a compromise.

[3] describes a design for a morphing helicopter blade. The chord in the morphable sections could be extended by 30% through a cellular structure and flexible skin material. The article presents structural design thoughts, like the adjustment of the skin and includes a finite element analysis to ensure the strains do not exceed the maximum allowable.This study is shown as a proof-of-concept for chord morphing with flexible skin materials using a honeycomb structure to support it.

[4] aimed to increase helicopter rotor performance in hover. The design variables included twist, taper ratio and initiation point, blade root chord and airfoil distribution function coefficients. An improvement in power and figure of merit was found to be achieveable with adjusted blade geometries compared to a baseline rotor.

The European project SABRE [5] is targeting a reduction of emissions with the research of several rotor blade morphing concepts, where the DLR Germany is represented by its variable chord extension concept [6] besides other morphing technologies.

A variable rotor geometry allows to adjust the rotor for optimal performance at each velocity. Helicopter rotors have been optimized with various optimization techniques.

[7] used a CONMIN algorithm to determine the best shape of a rotor blade, while [8] proofed genetic algorithms to be sufficient for rotor blade optimizations. [9] used a multi variable particle swarm optimization (PSO) and showed that the power of a rotor can be reduced significantly compared to a baseline profile. Another approach to optimize a helicopter rotor with a PSO in combination with a comprehensive analysis can be found in [10]. The PSO was found to be more ac-

curate than other evolutionary algorithms in this case. Genetic and PSO algorithms are both nature-oriented optimization methods, what can be beneficial depending on the optimization problem. There is no need for gradial information of the objective function, which is one main advantage compared to conventional mathematical approaches. Hence, there are often less function evaluations necessary to calculate a global optimum. A drawback for this type of optimizations is, that the solution is not necessarily the global optimum, since no gradient is evaluated. However, it is still the lowest value that was found within all function evaluations of the algorithm. Therefore, the quality of results is dependent on the problem definition and the selection of optimization parameters, like number of particles and the particle movement per iteration for the case of a PSO.

Since helicopters have unique abilities like vertical takeoff and landing, on the spot turning and hover flight, they are used for a variety of different missions which can have effect on the optimization.

The goal of this work is to find the optimal morphing parameters for a linearly chord morphing rotor concept, developed by the DLR. A full mission should be optimized to require less power than the baseline rotor model, while keeping structural and vibrational strains within boundaries. An optimization algorithm based on the work of [11] and [12] shall be implemented to achieve this goal.

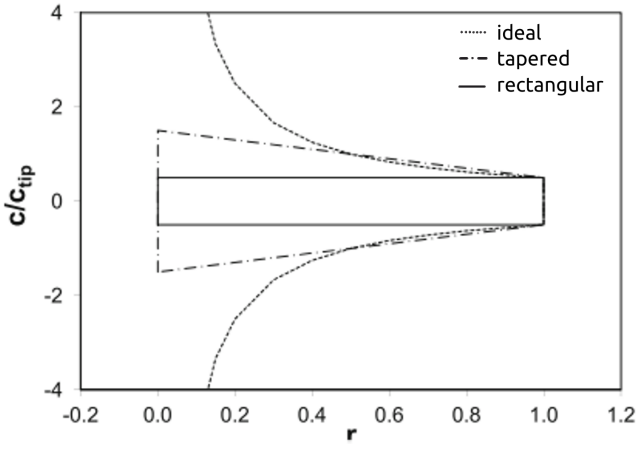

Figure 1: Rotor chord length over non dimensional rotor radius r

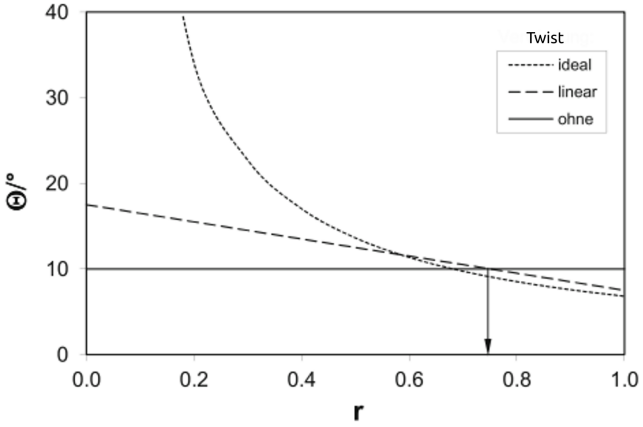

Figure 2: Rotor twist over non dimensional rotor radius r

MORPHING ROTOR BLADE

The variable chord extension concept uses a combination of an actuator and a hinge, which are located at the beginning of the aerodynamic profile of the blade and its trailing edge, respectively. The actuator can change the blade geometry by pushing the trailing edge further back. This is possible due to a changed airfoil structure which includes elastic skin components.

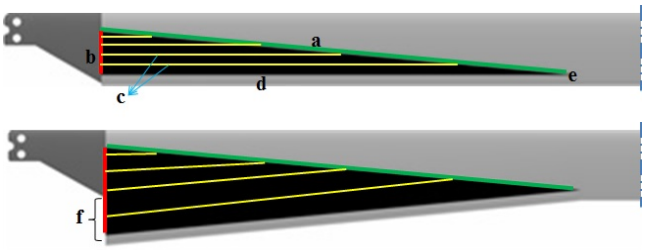

Figure 3: Unmorphed rotor blade (top) and the fully extended rotor blade with a) auxiliary spar(green), b) guidance system (red), c) web siffeners, d) read spar, e) hinge, f) maximum chord-extension Δc

The top view can be seen in Fig. 3, where the black area indicates the morphing section. The aforementioned actuator (b), the hinge (c) and the trailing edge spar (d) are shown in the graphic. Since soft skin material in used to allow a chord extension in this area, the airfoil geometry is supported by stiffeners (c). (f) shows the chord extension Δc of the morphed profile. The optimal hovering rotor also features a hyperbolical twisted blade shown in Fig. 2, which can be immitated by an additional deflection of the generated extension as shown in Fig. 4, where (a) shows the baseline blade, (b) shows a chord extension of 50% and (c) shows the extended blade including a deflection α_d (Figure adapted from Fig 3. in [6]).

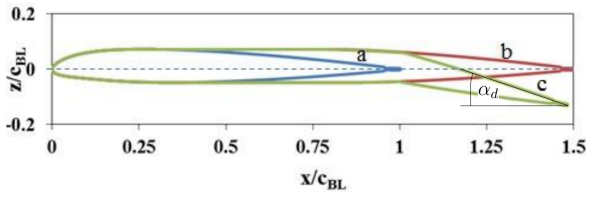

Figure 4: NACA23012tab airfoil with chord-extension and deflection. a) Baseline airfoil, b) with 50% chord extension Δc, c) with 50% chord extension Δc and deflection α_d

The chord extension Δc is measured in percent with respect to the baseline profile, the deflection α_d in degrees. The hinge location r_h is given in normalized radial coordinates and runs from 0 at the blade root to 1 at the tip.

When the rotor airfoil gets changed during flight, it changes the mechanical properties and mass distribution of the rotor. Therefore they have to be considered by the comprehensive analysis performing the rotor calculations. The software to trim the rotor is called S4. It is a DLR internal comprehensive analysis of rotorcraft which uses elastic blade models to simulate the helicopter rotor. The FEM model used by S4 to simulate the rotor is dependent on the radial location of the hinge and the extension of the blade. Different models covering a range between $r_h = 0.4$ to $r_h = 0.7$ have been created in steps of 0.05. The blade extension Δc is subdivided in steps of 12.5%. S4 always chooses the closest possible model for the structural analysis, while the aerodynamic calculations are continuous.

The Bo105 rotor blade was selected as a baseline rotor blade. It uses the NACA23012tab airfoil and has a rectangular blade gemoetry with 4.92m radius. The blade features a linear twist of -8 degrees. The rotor is powered by two engines with a total of 626kW.

Not every aspect of the morphing rotor blade is changeable during flight. Even if the extension and the deflection of the morphing section are able to change, the position of the hinge, the actuator and the structure behind the mechanism are fixed. Additionally, it is not sure which percentages of extension, deflection or even which position of the hinge will lead to the best power savings during flight. It is possible, that a hovering rotor favours a hinge located at $r_h = 0.4$ with full extension and deflection, while a rotor in forward flight conditions favours a hinge location of r=0.7 with minimal extension and deflection. Since the hinge location can not be changed during flight, it has to be set prior to manufacturing. Fixing the hinge position is not trivial, since multiple parameters have influence on the optimal position. To find out which location should be chosen, a multi-variable optimization has to be done. The optimization is dependent on the target mission, since it specifies the considered velocities.

MISSIONS

To observe if the mission type has effect on the optimal morphing parameters, a total of three missions are analyzed. The first mission describes a military scenario inspired by [13] as shown in Fig. 5, where the helicopter approaches the target area at high velocity, slows down and hovers while waiting for commands, before attacking and flying back to base at high velocities. The mission has long hover and low velocity phases, which are converted into weightage factors w_{vi}. The weightage factors are directly dependent on the time of the velocity during the whole mission and can be seen in Table 1, Table 2 and Table 3. The second mission is inspired by [14] and shown in Fig. 6. It describes a search and rescue mission where the helicopter is moving fast to the target area, before it is slowing down for the search / observation part, while hovering from time to time. When the mission is complete, it returns to base at high velocity. This mission is a balanced profile and includes low velocity and hover phases, as well as high velocities. The third mission is designed to have long high velocity phases as shown in Fig. 7. It is ment to be a transport mission with very short hover phase, where the helicopter is approaching to a target area fast, hovering for a short time and then returning to base at high velocity.

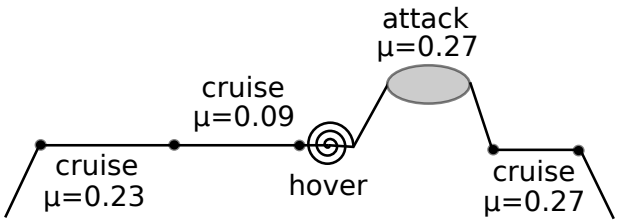

Figure 5: Mission 1: Military

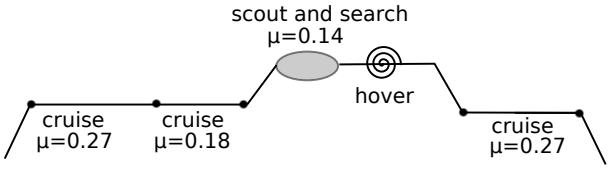

Figure 6: Mission 2: Search and rescue

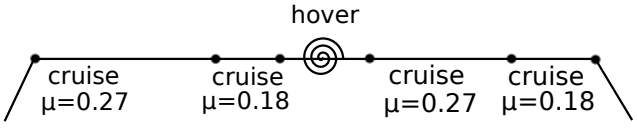

Figure 7: Mission 3: Transport

Table 1: Mission 1: Military

velocity$[\frac{m}{s}]$	$w_{vi}[\%]$	duration$[s]$	μ
0	25	1500	0
20	31	1796	0.09
50	13	718	0.23
60	31	1800	0.27

Table 2: Mission 2: Search and rescue

velocity$[\frac{m}{s}]$	$w_{vi}[\%]$	duration$[s]$	μ
0	12	120	0
30	24	250	0.14
40	12	120	0.18
60	52	530	0.27

Table 3: Mission 3: Transport

velocity$[\frac{m}{s}]$	$w_{vi}[\%]$	duration$[s]$	μ
0	7	60	0
40	29	240	0.18
60	64	530	0.27

OPTIMIZATION

The implemented optimization is a particle swarm algorithm. It has an iterative character and was developed for neural networks [15]. It is based on a swarm of particles which can be imagined as individual entities. Each of these particles P has knowledge of its position $\boldsymbol{x}_{P,i}$, velocity $\boldsymbol{v}_{P,i}$ and the objective function $f(\boldsymbol{x})$, which has to be minimized. It also knows the best objective value it ever calculated over all previous iterations i and the position $\boldsymbol{x}_{minP,i}$ to achieve it, alongside the current global best value including its position $\boldsymbol{x}_{minG,i}$. The global best value can be received through communication with the other particles. The global and particle best values are updated every time a particle finds a new minimum. The flowchart in Fig. 8 shows the general structure of a PSO. Initially, all particles are distributed across the search domain with a randomly (sometimes manually) chosen position $\boldsymbol{x}_{P,i}$, where i represents the current iteration. The second step is to evaluate the objective function for each particle at its current position $\boldsymbol{x}_{P,i}$, check if constraints are satisfied and update the personal and global minima $F_{minP,i}$ and $F_{minG,i}$ as shown in Fig. 9, before all particles can move to a new position. The next iteration is startet, if the cancel criterion, which decides if the optimization is complete, is not satisfied.

Figure 8: Flowchart: basic structure of a particle swarm algorithm

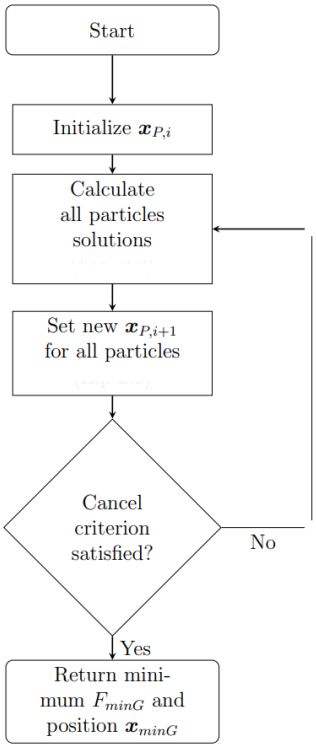

The update of the particle positions is required each iteration, where Eq. 1 and Eq. 2 [12] are used to generate new positions for each particle.

$$\boldsymbol{v}_{P,i+1} = h * \boldsymbol{v}_{P,i} + c_1 * \boldsymbol{r}_1 * (\boldsymbol{x}_{minP,i} - \boldsymbol{x}_{P,i}) + c_2 * \boldsymbol{r}_2 * (\boldsymbol{x}_{minG,i} - \boldsymbol{x}_{P,i}) \quad (1)$$

$$\boldsymbol{x}_{P,i+1} = \boldsymbol{x}_{P,i} + \boldsymbol{v}_{P,i+1} \quad (2)$$

Eq. 1 calculates the velocity $\boldsymbol{v}_{P,i+1}$ of each particle P. The velocity describes the change of the position per iteration. $\boldsymbol{r}_1$ and $\boldsymbol{r}_2$ are randomly generated factors ranging from 0 to 1, which differ for each particle and iteration. The constants h, c_1 and c_2 limit the influence of the current minima and the current velocity $\boldsymbol{v}_{P,i}$ on the new velocity. When the velocity for each particle is calculated, the positions $\boldsymbol{x}_{P,i}$ are updated as seen in Eq. 2. The optimization is considered complete (the cancel criterion is satisfied), if the global optimum $F_{minG,i}$ does not change over multiple iterations, or a maximum number of iterations has been evaluated.

Objectives

An objective is the target value of the optimization procedure. It has to be minimized and can be expressed with an objective function $f(\boldsymbol{x})$ in the optimization algorithm. Even with the main objective of the optimization being power efficiency, other additional objectives shall be taken into account.

Figure 9: Flowchart: Particle solution calculation

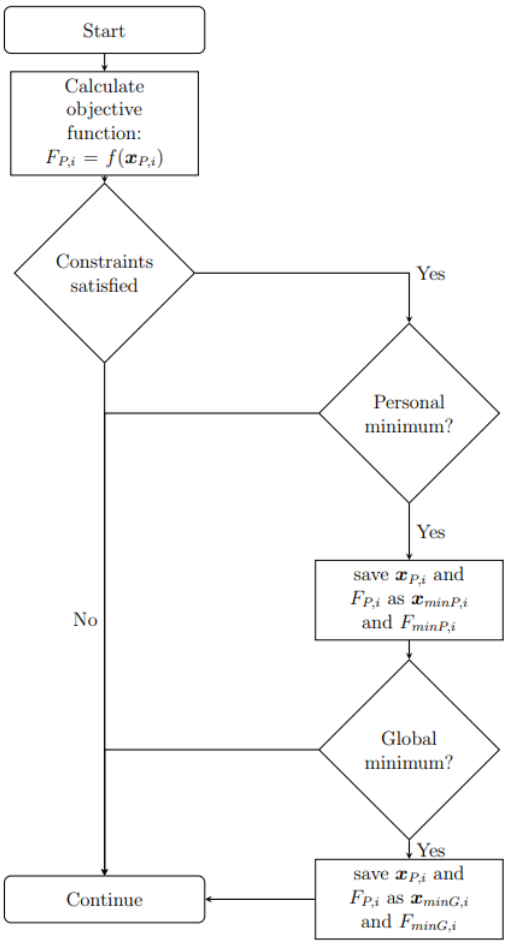

Besides the power consumption P of the helicopter rotor as primary objective, a structural and vibrational criterion represent secondary objectives. The blade tip elastic torsion Φ in degrees was chosen to be the structural criterion, since the soft skin of the morphing rotor blade provides less torsional stiffness. In terms of vibration, the N/rev vertical hub force $Fz_{4/rev}$ is used as an indicator. The so created multi objective problem is combined to a single total objective for the optimization algorithm. The combination is implemented as a linear combination of the normalized objectives multiplied with a weightage w_i per objective:

$$f(\boldsymbol{x}) = \sum \frac{O_i}{N_i} * w_i \tag{3}$$

A normalization with factors N_i shown in Table 4 is necessary due to the variable scale of the objective values O_i.

Table 4: Objective normalization factors

Objective O_i	N_i
P	350 kW
Φ	2.5°
$Fz_{4/rev}$	500 N

The vibrational and structural objectives are normalized with respect to the maximum constraints, which are described later. The normalization ensures a power objective in the region of one, while the normalized structural and vibrational objectives can vary in the range of 0 to 2.

Three different scenarios as seen in Table 5 were chosen to be observed in detail. Scenario (Sc.) 1 has the power consumption P as single objective, while Scenario 2 and 3 include Φ and $Fz_{4/rev}$, respectively.

Table 5: Scenario definition

w_i	Sc. 1	Sc. 2	Sc. 3
w_P	1	0.5	0.33
w_Φ	0	0.5	0.33
$w_{Fz_{4/rev}}$	0	0	0.33

Design Variables

The design variables of the morphing rotor blade can be considered as the position of each particle. Based on the chord morphing concept, the design variables are the chord extension Δc, deflection α_d and hinge location r_h. Since the range of the design variable is different as seen in Table 6, scaling factors shown in Table 7 are introduced. These scaling factors are multiplied with the constants c_1 and c_2 in Eq. 1 to adjust the particle movement per iteration and were determined empirically. The design variables can only be set within a raster of the stepsize d_{min}.

Table 6: Design variables

Design variable	Lower boundary	Upper boundary
α_d	0°	15°
Δc	0 %	100%
r_h	0.4	0.7

Table 7: Design variable scaling factors

Design variable	Scaling factor	d_{min}
α_d	2.00	1°
Δc	3.33	1%
r_h	0.20	0.02

Constraints

Constraints are conditions which have to be satisfied, otherwise the design is not accepted by the optimization algorithm. They can either be set due to design choices or be required to represent reality accurately. The first constraint requires the rotor to be trimmed, which is determined through a boolean expression of S4.

Table 8: Baseline values

Advance ratio [-]	velocity [m/s]	P_{BL} [kW]	Φ_{BL}	$Fz_{4/rev}$
0.00	0	369.89	0.455	17
0.05	10	307.58	0.420	99
0.09	20	238.21	0.433	594
0.14	30	229.77	0.530	734
0.18	40	255.37	0.676	629
0.23	50	309.87	0.884	473
0.27	60	402.59	1.151	371

The maximal power consumption of the blade has to be lower than the baseline (BL) profile (Table 8), while Φ and $Fz_{4/rev}$ have to stay within boundaries. The vibrational and structural constraints can be seen in Table 9. The constraints are set to higher values than the baseline rotor provides, since the stiffnesses of the morphing profile are different and higher elastic tip torsions are expected.

Table 9: Optimization constraints

	Constraint	
Power	P	$< P_{BL}$
Structural	Φ	$< 5°$
Vibrational	$Fz_{4/rev}$	$< 1000N$

Implementation

As mentioned before, the hinge can not be moved during flight. This has to be taken into account for the implementation of the optimization algorithm, since the whole mission can only be influenced by the change of Δc and α_d. Hence, the optimization is split up into two separate levels, where the first level L1 aims to find an optimal hinge position. For each particle in this first level L1, the mission has to be completed with the best available morph settings. This requires a second level L2 inside the particles objective function, which determines the best morph parameter combination for each velocity in the mission. The PSO can be used for both levels, but with different inputs as shown in Table 10.

Table 10: Levels of optimization

Level	Particles	Design variables $\boldsymbol{x}$	$f(\boldsymbol{x})$
L1	10	r_h	Eq. 4
L2	25	Δc, α_d	Eq. 3

Level	h	c_1	c_2
L1	0.4	0.1	0.1
L2	0.5	0.2	0.2

The first level has the aim to find the best possible objective (e.g. lowest power) over the whole mission. This is achieved by solving the L2 particle swarm optimization at each velocity v and combining the results as shown in Eq. 4.

$$f_{L1}(\boldsymbol{x}) = \sum_v F_{L2,v} * w_{vi} \tag{4}$$

w_{vi} is the weightage of velocity v (Table 1 to Table 3), while $F_{L2,v}$ represents the global optimum F_{minG} of the second level optimization L2 for velocity v. The second level optimization L2 uses Eq. 3 as objective function.

Due to the leveled structure of the optimization it is necessary to limit the amount of particle evaluations per iteration. Therefore, the particles are distributed equally at the beginning of each PSO, to cover the whole search domain with less particles.

An optimization is considered to be complete, if the global optimum does not change over three iterations, or a total of more than ten iterations were evaluated. h is also lowered by 17% of its current value each iteration to reduce particle movement over time.

Power savings P_s can be calculated with Eq. 5, where P_{BL} represents the baseline power consumption.

$$P_s = 1 - \frac{P}{P_{BL}} \tag{5}$$

The power saving of a total mission with velocities v is calculated as follows:

$$P_{s,mission} = \sum_v w_{vi} * P_s. \tag{6}$$

RESULTS

After running the optimization for the three missions in three different scenarios, the results can be plotted in graphs showing the total mission objective F, which is the personal best value F_{minP} of a particle in the first level L1. Scenario 1 considers power, the performance criterion, as only objective. Scenario 2 additionally includes Φ as structural criterion, which represents the blade tip elastic torsion in degrees, while Scenario 3 also adds $Fz_{4/rev}$ as the vibrational criterion. Φ and $Fz_{4/rev}$ are ignored by the optimization algorithm if they are not used for the objective calculation, but are displayed in all tables for comparison purposes. It has to be noted, that the axes for Scenario 2 and 3 are identical, while Scenario 1 shows a different region. This is necessary to make the trend of the individual Scenarios clearly visible.

Scenario 1

Fig. 10, Fig. 11 and Fig. 12 all show a clear trend towards hinge locations close to the blade tip, where the optima can be found at $r_h = 0.64$ for all three missions. Table 11, Table 13 and Table 15 show the morph parameters, which were found to be the most beneficial for this scenario. As expected, due to the optimal hovering rotor, Δc is very high for low velocities and hover, while getting lower with a rising advance ratio. It can also be noticed, that Φ is higher than for the baseline profile,

especially with an extended blade. The blade deflection α_d was found to be disadvantageous for all cases, since it creates values for Φ and $Fz_{4/rev}$, which do not satisfy the constraints and are therefore not accepted by the optimization algorithm. Table 12 shows, that the power consumption could be reduced by a total of up to 5.58% compared to the baseline rotor, with an increase in elastic blade tip torsion. Mission 1 shows the best total power saving potential, which can be traced back to the velocity distribution in the missions. The long low velocity an hover phases create the highest potential for power savings across all three missions as shown in Table 12, Table 14 and Table 16, where mission 1, 2 and 3 could save a total of $P_{s,1} = 5.58\%$, $P_{s,2} = 4.26\%$ and $P_{s,3} = 3.64\%$, respectively.

Scenario 2

Fig. 13, Fig. 14 and Fig. 15 show a trend towards hinge locations close to the blade root, where the optima can be found at $r_h = 0.44$ for missions 1 and 3 and $r_h = 0.54$ for mission 2. The total mission objective increases with the weightage of high velocity phases from minima of $F_{minP} = 0.67$ to $F_{minP} = 0.77$. Table 17, Table 19 and Table 21 show a significant decrease in Φ compared to scenario 1, due to the selection of objectives. It is also noticable, that the overall trend shows less Δc and negligible values of α_d. Mission 2 shows a high Δc for $\mu = 0.18$ as optimum, which creates high vibrations while keeping P and the mean elastic blade tip torsion Φ low. Scenario 2 also has the optimal hinge position at $r_h = 0.54$, which can be explained with this value. Otherwise, the vibrations do not show significant changes compared to the baseline rotor. The overall power savings with respect to the baseline rotor are lower than in scenario 1, which can be explained with the additional focus on the blade tip elastic torsion Φ as secondary objective. The power savings per velocity can be seen in Table 18, Table 20 and Table 22. They range from $P_{s,2} = 1.64\%$ for mission 2, to $P_{s,1\&3} = 0.44\%$ for missions 1 and 3. The power improvements of mission 2 can be explained with the different positioning of the hinge along the rotor blade, which allows a larger blade area and can cause less power for the hovering rotor. It also changes the structural properties of the rotor, which appears to be beneficial for the power consumption in high velocity flight at $\mu = 0.27$.

Scenario 3

Fig. 16, Fig. 17 and Fig. 18 show a trend towards hinge locations close to the root like in scenario 2. The overall optima are found at $r_h = 0.44$ for mission 1, $r_h = 0.42$ for mission 2, and $r_h = 0.40$ for mission 3. The minimal objective value F_{minP} is increasing with the weightage of high advance ratios from $F_{minP} = 0.67$ for mission 1 to $F_{minP} = 0.76$ for mission 3. Table 23, Table 25 and Table 27 show the optimal settings for each mission, where a general trend to low values Δc and negligible values α_d can be observed. The vibrations indicated by $Fz_{4/rev}$ are generally lower than for the baseline rotor as seen in Table 8 for the most part, but are still in the same regions. P and Φ did not change significantly compared to scenario 2, except for mission 2, where the reduction of Δc causes a noticeable difference in $Fz_{4/rev}$ and Φ. The power savings per velocity in Table 24, Table 26 and Table 28 show no significant improvements compared to the baseline rotor, with values from $P_{s,2} = 0.10\%$ in mission 2, $P_{s,3} = 0.11\%$ in mission 3 and $P_{s,1} = 0.51\%$ in mission 1. This can be explained with the additional focus on $Fz_{4/rev}$ and Φ. The best power savings can be observed at high velocities for $r_h = 0.44$ in mission 1, but they are still in regions below 0.8% at all and below 0.2% most of the time.

Summary

In summary, the optimization was shown to be successful for all three scenarios. The power could be reduced for up to $P_{s,mission} = 5.58\%$ with respect to the baseline rotor, while an increase in power efficiency created higher structural and vibrational strains. The power efficiency increases with a further outside located hinge, which results in larger possible blade areas and less torsional stiffness than the baseline rotor. Hence, larger elastic blade tip torsion Φ has to be considered for blade chord extensions Δc of up to 100% for hover and low velocity flight. The blade deflection α_d was shown to be disadvantageous for all scenarios, due to high values of Φ and $Fz_{4/rev}$ which did not satisfy the constraints. Scenarios 2 and 3 favour hinges located close to the beginning of the aerodynamic section of the blade from $r_h = 0.40$ to $r_h = 0.54$, which can be explained with the change in structural properties which has effect on the secondary objectives. The weightage of the secondary objectives has also influence on the power consumption, which is found to be very close to the baseline rotor for both scenarios. Hence, the power savings were found to be in regions below $P_{s,mission} = 1\%$ for almost every mission of scenario 2 and 3. Δc and α_d were found to be very small for all velocities.

The optimal morphing parameters for a power efficient rotor bade, that keeps vibrational and structural strains within boundaries, can be summarized as follows:

- $\uparrow \Delta c$ at low velocities
- $\downarrow \Delta c$ at high velocities
- $\downarrow \alpha_d$ at all times
- r_h close to the rotor tip

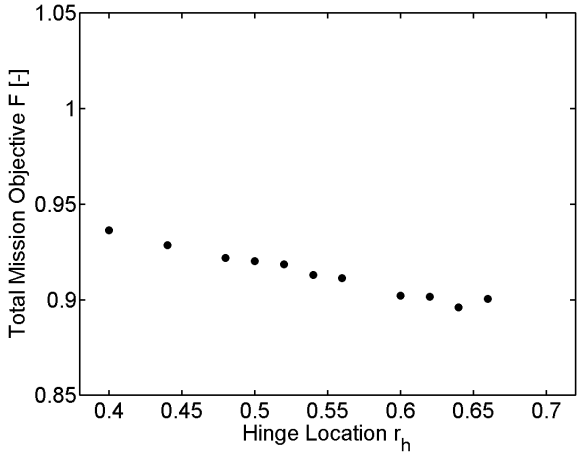

Figure 10: Mission 1, scenario 1: Total mission objective F over hinge location r_h

Table 11: Mission1 Scenario 1

μ [−]	Δ_c [%]	r_h [-]	α_d [°]	P [kW]	Φ [°]	$Fz_{4/rev}$ [N]
0.00	1.000	0.640	0.000	344.530	4.723	20.000
0.09	1.000	0.640	0.000	220.440	4.379	492.000
0.23	0.000	0.640	0.000	301.230	1.606	507.000
0.27	0.000	0.640	0.000	387.090	1.952	292.000

Table 12: Mission1 Scenario 1: power savings

μ [−]	P [kW]	P_{BL} [kW]	P_s [%]
0.00	344.530	369.890	6.856
0.09	220.440	238.210	7.460
0.23	301.230	309.870	2.788
0.27	387.090	402.590	3.850

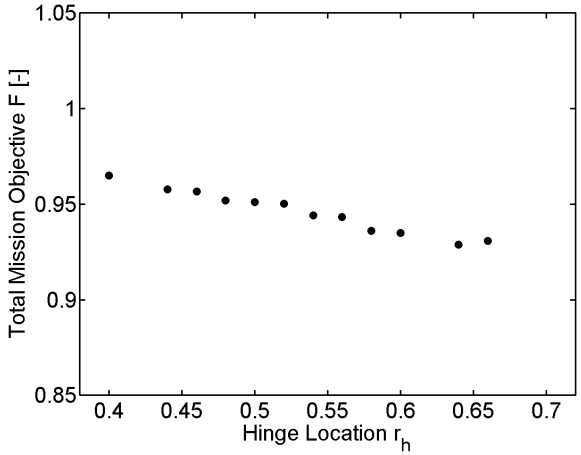

Figure 11: Mission 2, scenario 1: Total mission objective F over hinge location r_h

Table 13: Mission2 Scenario 1

μ [−]	Δ_c [%]	r_h [-]	α_d [°]	P [kW]	Φ [°]	$Fz_{4/rev}$ [N]
0.00	1.000	0.640	0.000	344.530	4.723	20.000
0.14	1.000	0.640	0.000	218.910	4.460	556.000
0.18	0.060	0.640	0.000	249.030	1.463	694.000
0.27	0.000	0.640	0.000	387.090	1.952	292.000

Table 14: Mission2 Scenario 1: power savings

μ [−]	P [kW]	P_{BL} [kW]	P_s [%]
0.00	344.530	369.890	6.856
0.14	218.910	229.770	4.726
0.18	249.030	255.370	2.483
0.27	387.090	402.590	3.850

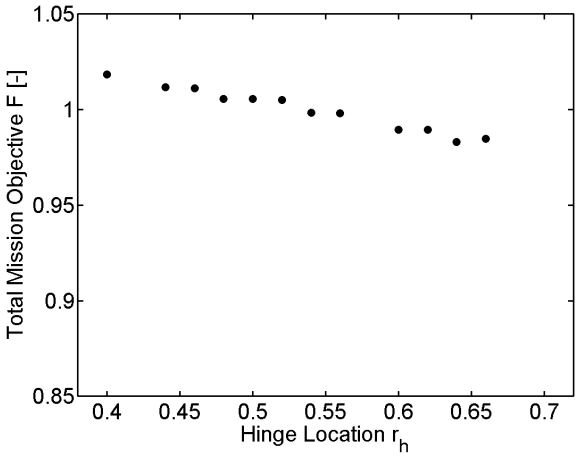

Figure 12: Mission 3, scenario 1: Total mission objective F over hinge location r_h

Table 15: Mission3 Scenario 1

μ [−]	Δ_c [%]	r_h [-]	α_d [°]	P [kW]	Φ [°]	$Fz_{4/rev}$ [N]
0.00	1.000	0.640	0.000	344.530	4.723	20.000
0.18	0.000	0.640	0.000	249.220	1.358	695.000
0.27	0.000	0.640	0.000	387.090	1.952	292.000

Table 16: Mission3 Scenario 1: power savings

μ [−]	P [kW]	P_{BL} [kW]	P_s [%]
0.00	344.530	369.890	6.856
0.18	249.220	255.370	2.408
0.27	387.090	402.590	3.850

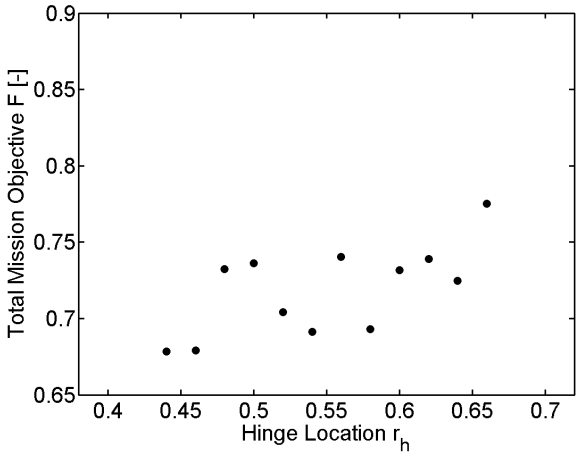

Figure 13: Mission 1, scenario 2: Total mission objective F over hinge location r_h

Table 17: Mission1 Scenario 2

μ [−]	Δ_c [%]	r_h [-]	α_d [°]	P [kW]	Φ [°]	$Fz_{4/rev}$ [N]
0.00	0.060	0.440	0.000	369.450	0.766	20.000
0.09	0.040	0.440	0.000	237.390	0.704	550.000
0.23	0.040	0.440	0.000	308.160	1.192	441.000
0.27	0.060	0.440	0.000	399.560	1.518	324.000

Table 18: Mission1 Scenario 2: power savings

μ [−]	P [kW]	P_{BL} [kW]	P_s [%]
0.00	369.450	369.890	0.119
0.09	237.390	238.210	0.344
0.23	308.160	309.870	0.552
0.27	399.560	402.590	0.753

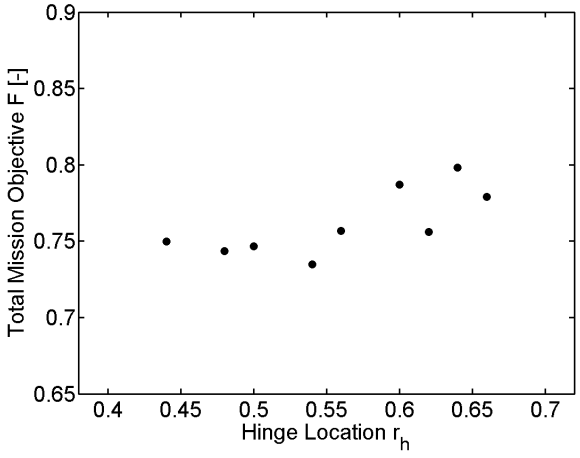

Figure 14: Mission 2, scenario 2: Total mission objective F over hinge location r_h

Table 19: Mission2 Scenario 2

μ [−]	Δ_c [%]	r_h [-]	α_d [°]	P [kW]	Φ [°]	$Fz_{4/rev}$ [N]
0.00	0.820	0.540	0.000	360.860	0.315	43.000
0.14	0.060	0.540	0.000	227.180	1.070	745.000
0.18	0.880	0.540	1.000	255.020	0.255	948.000
0.27	0.100	0.540	0.000	394.350	1.860	295.000

Table 20: Mission2 Scenario 2: power savings

μ [−]	P [kW]	P_{BL} [kW]	P_s [%]
0.00	360.860	369.890	2.441
0.14	227.180	229.770	1.127
0.18	255.020	255.370	0.137
0.27	394.350	402.590	2.047

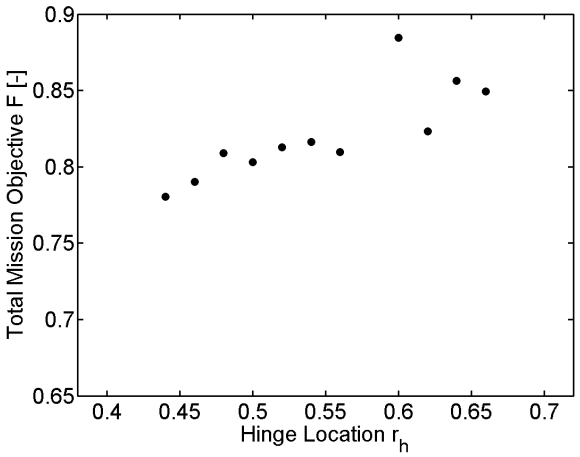

Figure 15: Mission 3, scenario 2: Total mission objective F over hinge location r_h

Table 21: Mission3 Scenario 2

μ [−]	Δ_c [%]	r_h [-]	α_d [°]	P [kW]	Φ [°]	$Fz_{4/rev}$ [N]
0.00	0.140	0.440	0.000	367.870	0.821	19.000
0.18	0.020	0.440	1.000	255.030	1.033	578.000
0.27	0.160	0.440	0.000	400.280	1.567	334.000

Table 22: Mission3 Scenario 2: power savings

μ [−]	P [kW]	P_{BL} [kW]	P_s [%]
0.00	367.870	369.890	0.546
0.18	255.030	255.370	0.133
0.27	400.280	402.590	0.574

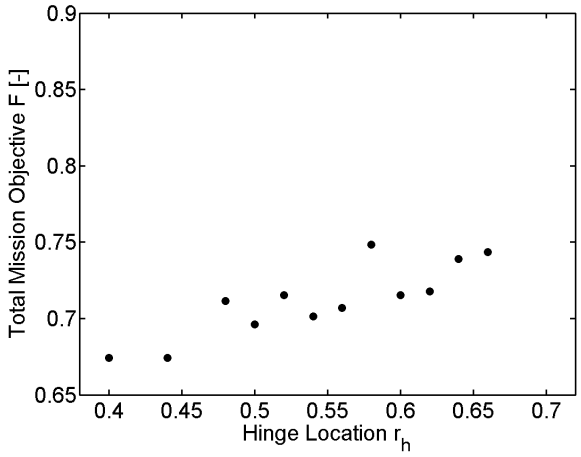

Figure 16: Mission 1, scenario 3: Total mission objective F over hinge location r_h

Table 23: Mission1 Scenario 3

μ [−]	Δ_c [%]	r_h [-]	α_d [°]	P [kW]	Φ [°]	$Fz_{4/rev}$ [N]
0.00	0.100	0.440	0.000	369.060	0.795	19.000
0.09	0.080	0.440	0.000	237.150	0.728	549.000
0.23	0.020	0.440	0.000	308.130	1.181	441.000
0.27	0.020	0.440	0.000	399.420	1.496	321.000

Table 24: Mission1 Scenario 3: power savings

μ [−]	P [kW]	P_{BL} [kW]	P_s [%]
0.00	369.060	369.890	0.224
0.09	237.150	238.210	0.445
0.23	308.130	309.870	0.562
0.27	399.420	402.590	0.787

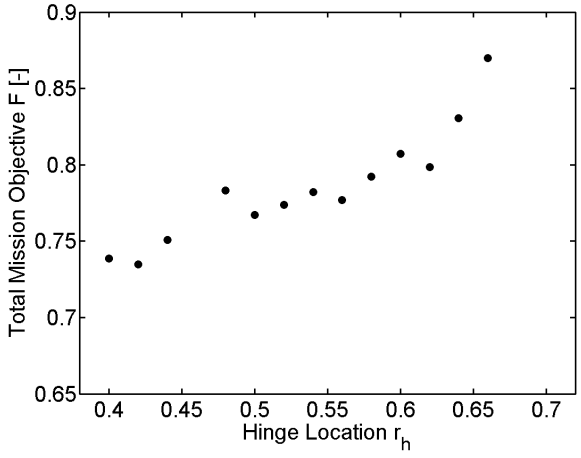

Figure 17: Mission 2, scenario 3: Total mission objective F over hinge location r_h

Table 25: Mission2 Scenario 3

μ [−]	Δ_c [%]	r_h [-]	α_d [°]	P [kW]	Φ [°]	$Fz_{4/rev}$ [N]
0.00	0.060	0.420	0.000	369.780	0.657	18.000
0.14	0.200	0.420	0.000	229.640	0.807	643.000
0.18	0.000	0.420	0.000	255.230	0.845	568.000
0.27	0.000	0.420	0.000	401.970	1.370	338.000

Table 26: Mission2 Scenario 3: power savings

μ [−]	P [kW]	P_{BL} [kW]	P_s [%]
0.00	369.780	369.890	0.030
0.14	229.640	229.770	0.057
0.18	255.230	255.370	0.055
0.27	401.970	402.590	0.154

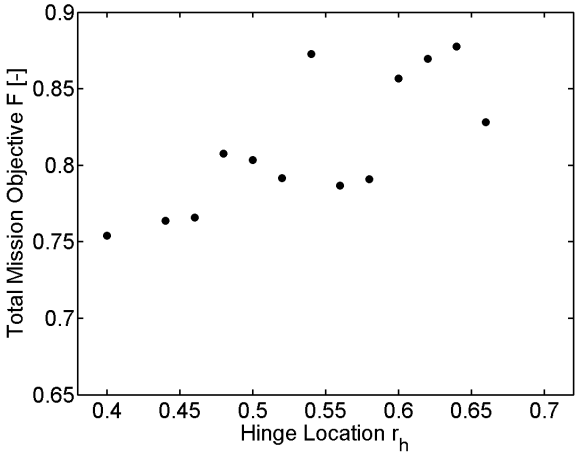

Figure 18: Mission 3, scenario 3: Total mission objective F over hinge location r_h

Table 27: Mission3 Scenario 3

μ [−]	Δ_c [%]	r_h [-]	α_d [°]	P [kW]	Φ [°]	$Fz_{4/rev}$ [N]
0.00	0.120	0.400	1.000	369.360	0.717	18.000
0.18	0.220	0.400	0.000	255.280	0.954	550.000
0.27	0.040	0.400	0.000	402.040	1.383	340.000

Table 28: Mission3 Scenario 3: power savings

μ [−]	P [kW]	P_{BL} [kW]	P_s [%]
0.00	369.360	369.890	0.143
0.18	255.280	255.370	0.035
0.27	402.040	402.590	0.137

CONCLUSION

A particle swarm optimization has been implemented and used for multi objective performance optimization

of three missions through a chord morphing rotor concept, which is currently in development by the DLR for project SABRE. The optimization problem was split into two levels, which was required due to the morphing mechanism and mission structures. Power improvements of up to 5.58% with respect to the baseline rotor were found to be possible with compromises in other disciplines like hub vibrations and elastic blade tip torsion, due to changed structural parameters. With the inclusion of secondary objectives, the power savings with respect to the baseline rotor were reduced. The objective weightages can be adjusted to further reduce the rotor power comsumption for multi objective optimizations in the future and more design variables or other rotor morphing concepts can be included.

REFERENCES

[1] A. Gessow, "Effect of rotor-blade twist and planform taper on helicopter hovering performance," *NACA TN 1542*, 1948.

[2] B. G. van der Wall, *Grundlagen der Hubschrauber-Aerodynamik*, p. 198. Berlin,Heidelberg: Springer Berlin Heidelberg, 2015.

[3] S. Barbarino, F. Gandhi, and S. D. Webster, "Design of extendable chord sections for morphing helicopter rotor blades," *Journal of Intelligent Material Systems and Structures*, vol. 22, no. 9, pp. 891–905, 2011.

[4] N. A. Vu, H.-J. Kang, A. I. Azamatov, J.-W. Lee, and Y.-H. Byun, "Aerodynamic design optimization of helicopter rotor blades in hover performance using advanced configuration generation method," 35th European Rotorcraft Forum 2009, Hamburg, Germany, 2009.

[5] J. Rauleder, B. G. van der Wall, A. Abdelmoula, D. Komp, S. Kumar, V. Ondra, B. Titurus, and B. K. Woods, "Aerodynamic performance of morphing blades and rotor systems," AHS International 74th Annual Forum & Technology Display, Phoenix, Arizona, 2018.

[6] R. K. Majeti, B. G. van der Wall, and C. G. Balzarek, "Linearly variable chord-extension morphing for helicopter rotor blades," The Vertical Flight Society's 75th Annual Forum & Technology Display, 2019.

[7] J. L. Walsh, "Performance optimization of helicopter rotor blades," *NASA TM-104054*, 1991.

[8] A. Massaro, A. D'Andrea, and E. Benini, "Multiobjective-multipoint rotor blade optimization in forward flight conditions using surrogate-assisted memetic algorithms," 37th European Rotorcraft Forum, 2011.

[9] R. Ramanujam and A. Abhishek, "Performance optimization of variable-speed and variable-geometry rotor concept," *Journal of Aircraft*, vol. 54, no. 2, pp. 476–489, 2016.

[10] G. Guglieri, "Using of particle swarm for performance optimization of helicopter rotor blades," *Applied Mathematics*, vol. 3, no. 10, p. 1403, 2012.

[11] J. Kennedy and R. C. Eberhart, "Particle swarm optimization," pp. 1942–1948, Proc. IEEE Int'l. Conf. on Neural Networks, 2019.

[12] S. K. Mishra, "Performance of repulsive particle swarm method in global optimization of some important test functions: A fortran program," in *Available at SSRN 924339*, Available Online: `http://www.ssrn.com/abstract=924339`, 2006.

[13] W. A. Crossley and D. H. Laananen, "Conceptual design of helicopters via genetic algorithm," *Journal of Aircraft*, vol. 33, no. 6, pp. 1062–1070, 1996.

[14] K. Karamolegkos, I. Goulos, V. Pachidis, J. Stevens, C. Smith, L. Thevenot, and R. d'Ippolito, "Helicopter mission analysis using a multidisciplinary simulation framework," American Society of Mechanical Engineers, ASME Turbo Expo 2014: Turbine Technical Conference and Exposition, 2014.

[15] J. Kennedy, "The particle swarm: social adaptation of knowledge," pp. 303–308, IEEE, Proceedings of 1997 IEEE International Conference on Evolutionary Computation (ICEC'97), Piscataw, NJ, 1997.